Theoretical Studies of Inorganic and Organometallic Reaction Mechanisms. 12. Intramolecular Carbon−Hydrogen Bond Activation in (Butenyl)manganese Tricarbonyl

Julie L. C. Thomas and Michael B. Hall*

Department of Chemistry, Texas A&M University, College Station, Texas 77843-3255

Received February 18, 1997[⊗]

Theoretical treatment of the fluxional behavior exhibited by (butenyl)manganese tricarbonyl, $(C_4H_7)Mn(CO)_3$, is challenging because the structure contains a first-row transition metal and an agostic interaction between the butenyl fragment and the manganese center. $(C_4H_7)Mn(CO)_3$ displays two fluxional processes on the NMR time scale. The first averages the hydrogens on the agostic carbon and has an activation free energy of $\Delta G^{\ddagger} = 9.1$ kcal/mol. We have identified the transition state in this process and calculated an activation free energy of $\Delta G^{\ddagger}_{\text{theor}} = 8.43$ kcal/mol. In the transition state structure, the agostic bond is broken and the methyl group rotated. The second process averages the two halves of the *syn*-butadiene fragment and has an activation free energy of $\Delta G^{\ddagger} = 17.1$ kcal/mol. We have identified the transition state and intermediate structures for this process in which the agostic hydrogen oxidatively adds to the metal center. The calculated free energy of activation is $\Delta G^{\ddagger}_{\text{theor}} = 17.2$ kcal/mol. Geometries for the ground state, intermediate, and transition states were optimized at the Møller−Plesset second order perturbation theory and/or density functional theory (DFT) levels. The density functional results were superior to those obtained by MP2. Final energetics were calculated by quadratic configuration interaction on the DFT geometries in a basis set that contains polarization functions, with corrections for zero-point energy and temperature.

Introduction

For electron-rich, late transition metals, alkane activation typically proceeds *via* oxidative addition of a C−H bond in the substrate to the metal center, as in eq 1. Further chemistry can then be performed on the

$$M + R{-}H \rightarrow R{-}M{-}H \qquad (1)$$

alkyl substituent. The first activation of a free alkane by a transition metal complex was reported in 1982.[1] Initial photoproducts of both iridium and rhodium species, believed to be Cp*ML (L = CO, PPh_3, PMe_3, and M = Rh, Ir), were observed to cleave C−H bonds in alkanes. Since this work was reported, there has been a tremendous amount of research conducted into the mechanism and utilization of this reactivity.[2−4]

Interactions between C−H bonds and metal centers were first observed in the late 1960s and early 1970s[5] when several groups reported unusually close distances between an unsaturated metal center and the C−H bond of a ligand. Studies of metal−alkyl complexes, especially the so-called agostic complexes, in which electron donation from a C−H bond serves to fill a vacant coordination site on the metal, have been of particular interest,[6] as this could be viewed as a form of precoordination of an alkyl substrate prior to its

[⊗] Abstract published in *Advance ACS Abstracts,* May 1, 1997.

(1) (a) Janowicz, A. H.; Bergman, R. G. *J. Am. Chem. Soc.* **1982**, *104*, 352. (b) Hoyano, J. K.; Graham, W. A. G. *J. Am. Chem. Soc.* **1982**, *104*, 3723. (c) Crabtree, R. H.; Mellea, M. F.; Mihelsie, J. M.; Quick, J. M. *J. Am. Chem. Soc.* **1982**, *104*, 107. (d) Jones, W. D.; Feher, F. J. *J. Am. Chem. Soc.* **1982**, *104*, 4240.

(2) (a) Crabtree, R. H. *Chem. Rev.* **1995**, *95*, 987. (b) Partridge, M. G.; McCamley, A.; Perutz, R. N. *J. Chem. Soc., Dalton Trans.* **1994**, 3519. (c) Chin, R. M.; Dong, L.; Duckett, S. B.; Partridge, M. G.; Jones, W. D.; Perutz, R. N. *J. Am. Chem. Soc.* **1993**, *115*, 7685 and references therein. (d) Bianchini, C.; Barbara, P.; Meli, A.; Peruzzini, M.; Vacca, A.; Vizza, F. *Organometallics* **1993**, *12*, 2505. (e) Stang, P. J.; Cao, D. *Organometallics* **1993**, *12*, 996. (f) Quignard, F.; Lécuyer, C.; Choplin, A.; Olivier, D.; Basset, J.-M. *J. Mol. Catal.* **1992**, *74*, 353. (g) Sakakura, T.; Sodeyama, T.; Sasaki, K.; Wada, K.; Tanaka, M. *J. Am. Chem. Soc.* **1990**, *112*, 7221. (h) Jones, W. D.; Feher, F. J. *J. Am. Chem. Soc.* **1985**, *107*, 620.

(3) (a) Stoutland, P. O.; Bergman, R. G.; Nolan, S. P.; Hoff, C. D. *Polyhedron* **1988**, *7*, 1429. (b) Weiller, B. H.; Wasserman, E. P.; Bergman, R. G.; Moore, C. B.; Pimentel, G. C. *J. Am. Chem. Soc.* **1989**, *111*, 8288. (c) Wasserman, E. P.; Moore, C. B.; Bergman, R. G. *Science* **1992**, *255*, 315. (d) Schultz, R. H.; Bengali, A. A.; Tauber, M. J.; Weiller, B. H.; Wasserman, E. P.; Kyle, K. R.; Moore, C. B.; Bergman, R. G. *J. Am. Chem. Soc.* **1994**, *116*, 7369. (e) Bengali, A. A.; Schultz, R. H.; Moore, C. B.; Bergman, R. G. *J. Am. Chem. Soc.* **1994**, *116*, 9585. (f) Lian, T.; Bromberg, S. E.; Yang, H.; Proulx, G.; Bergman, R. G.; Harris, C. B. *J. Am. Chem. Soc.* **1996**, *118*, 3769. (g) Luecke, H. F.; Arndtsen, B. A.; Burger, P.; Bergman, R. G. *J. Am. Chem. Soc.* **1996**, *118*, 2517. (h) Bromberg, S. E.; Lian, T. Q.; Bergman, R. G.; Harris, C. B. *J. Am. Chem. Soc.* **1996**, *118*, 2069. (i) Arndtsen, B. A.; Bergman, R. G. *J. Organomet. Chem.* **1995**, *504*, 143. (j) Arndtsen, B. A.; Bergman, R. G. *Science* **1995**, *270*, 1970.

(4) (a) Esteruelas, M. A.; Lahoz, F. J.; Onate, E.; Oro, L. A.; Sole, E. *J. Am. Chem. Soc.* **1996**, *118*, 89. (b) Grubbs, R. H.; Coates, G. W. *Acc. Chem. Res.* **1996**, *29*, 85. (c) Duchateau, R.; Vanwee, C. T.; Teuben, J. H. *Organometallics* **1996**, *15*, 2291. (d) Purwoko, A. A.; Lees, A. J. *Inorg. Chem.* **1996**, *35*, 675. (e) Purwoko, A. A.; Lees, A. J. *J. Organomet. Chem.* **1995**, *504*, 107. (f) Purwoko, A. A.; Lees, A. J. *Inorg. Chem.* **1995**, *34*, 424. (g) Perutz, R. N.; Belt, S. T.; McCamley, A.; Whittlesey, M. K. *Pure Appl. Chem.* **1990**, *62*, 1539. (h) Perutz, R. N. *Pure Appl. Chem.* **1990**, *62*, 1103. (i) Brough, S. A.; Hall, C.; McCamley, A.; Perutz, R. N.; Stahl, S.; Wecker, U.; Werner, H. *J. Organomet. Chem.* **1995**, *504*, 33.

(5) (a) Bailey, N. A.; Jenkins, J. M.; Mason, R.; Shaw, B. L. *J. Chem. Soc., Chem. Commun.* **1965**, 237. (b) LaPlaca, S. J.; Ibers, J. A. *Inorg. Chem.* **1965**, *4*, 778. (c) Muir, K. W.; Ibers, J. A. *Inorg. Chem.* **1970**, *9*, 440. (d) Trofimenko, S. *J. Am. Chem. Soc.* **1968**, *90*, 4754. (e) Trofimenko, S. *Inorg. Chem.* **1970**, *9*, 2493. (f) Cotton, F. A.; Stanislowski, A. G. *J. Am. Chem. Soc.* **1974**, *96*, 5074. (g) Cotton, F. A.; Stanislowski, A. G. *J. Am. Chem. Soc.* **1974**, *96*, 754. (h) Cotton, F. A.; Day, V. W. *J. Chem. Soc., Chem. Commun.* **1974**, 415.

S0276-7333(97)00122-2 CCC: $14.00

oxidative addition, as shown in eq 2. Strong precoordination of the incoming group is often indicative of a more exothermic reaction system, compared to systems that do not exhibit precoordination. This greater exothermicity can lower the barrier for oxidative addition.

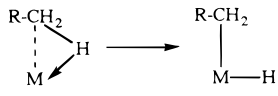

(2)

Agostic complexes have also been observed as the resting states in catalytic systems, where they are more stable than their metal-hydride isomers. For example, $[Cp^*Co\{P(OMe_3)\}(\eta^2\text{-Et})]^+$, an ethylene polymerization catalyst, has an agostic resting state.[7] The agostic interaction between the metal center and a carbon−hydrogen bond on the growing hydrocarbon chain may lower the barrier for the migratory insertion of the olefin in the course of the cycle.

A fluxional system that also has an agostic resting state is (butenyl)manganese tricarbonyl, $(C_4H_7)Mn(CO)_3$ (**1**). On the basis of the NMR spectroscopy, Brookhart

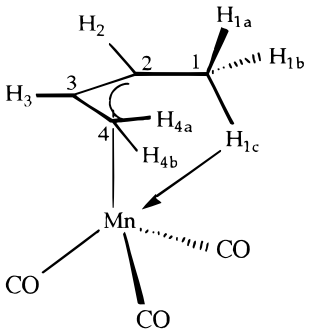

1. Agostic $(C_4H_7)Mn(CO)_3$

and co-workers proposed[8] that $(C_4H_7)Mn(CO)_3$ exists as an agostic complex in its ground state, but displays two fluxional processes observable on the NMR time scale. For the lower energy process ($\Delta G^{\ddagger} = 9.1$ kcal/mol), the NMR spectrum shows broadening of the peaks assigned to H_{1a-c} while the rest of the hydrogen peaks remain unperturbed. This indicates that scrambling among these three hydrogens is occurring. In the proposed mechanism for this first process, Scheme 1, the agostic bond between H_{1a} and the Mn center is broken (**2** in Scheme 1) and the methyl group rotates. The agostic bond reforms with another hydrogen on C_1. At a slightly higher energy ($\Delta G^{\ddagger} = 17.1$ kcal/mol), averaging occurs between the hydrogens on both ends of the butenyl fragment (H_{1a-c} and $H_{4a,b}$) as well as between H_2 and H_3, C_1 and C_4, and C_2 and C_3. This observation could be explained by the agostic hydrogen oxidatively adding to the Mn center and forming an η^4-butadiene complex (**3** in Scheme 2). The hydrogen could then add

Scheme 1

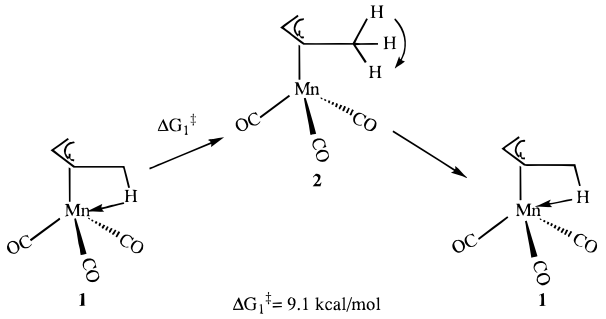

back to either end of the C_4 fragment and reform an agostic complex (Scheme 2.)

A related complex, $(CH_3C_6H_8)Mn(CO)_3$ (**5**), for which a crystal structure of the agostic ground state is known, showed similar behavior in a variable-temperature NMR study.[9] This behavior has been interpreted as involving two processes similar those shown in Schemes 1 and 2. Exchange between the *endo*-hydrogens that

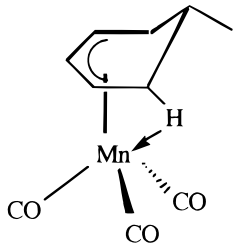

5. $(CH_3C_6H_8)Mn(CO)_3$

form the agostic bond on either side of the ring has an activation free energy ($\Delta G^{\ddagger}$) of 8.3 kcal/mol; formation of an η^4-cyclohexadiene complex, with the agostic hydrogen fully added to the metal center, has an activation free energy ($\Delta G^{\ddagger}$) of 15.4 kcal/mol.

Theoretical work has also been performed in an effort to understand more fully the behavior of both the alkanes and metal centers.[10,11] Early work concerning hydrogen activation by Vaska-type complexes was performed in this group by Sargent and Hall.[12a,b] Song and Hall also examined the activation of methane by CpRh-

(6) (a) Brookhart, M.; Green, M. L. H.; Wong, L-L. *Prog. Inorg. Chem.* **1988**, *30*, 1. (b) Brookhart, M.; Hauptman, E.; Lincoln, D. M. *J. Am. Chem. Soc.* **1992**, *114*, 10394. (c) Brookhart, M.; Lincoln, D. M.; Volpe, A. F., Jr.; Schmidt, G. F. *Organometallics* **1989**, *8*, 1212. (d) Brookhart, M.; Lincoln, D. M.; Bennett, M. A. *J. Am. Chem. Soc.* **1990**, *112*, 2691.

(7) (a) Crackness, R. B.; Orpen, A. G.; Spencer, J. L. *J. Chem. Soc., Chem. Commun.* **1984**, 326. (b) Brookhart, M.; Schmidt, G. F.; Lincoln, D.; Rivers, D. S. *Transition Metal Catalyzed Polymerizations*; Quirk, R., Ed.; Cambridge University Press: New York, 1988. (c) Schmidt, G. F.; Brookhart, M. *J. Am. Chem. Soc.* **1985**, *107*, 1443.

(8) Brookhart, M.; Noh, S. K.; Timmers, F. J. *Organometallics* **1987**, *6*, 1829.

(9) (a) Lamanna, W.; Brookhart, M. *J. Am. Chem. Soc.* **1981**, *103*, 989. (b) Brookhart, M.; Lamanna, W.; Humphery, M. B. *J. Am. Chem. Soc.* **1982**, *104*, 2117. (c) Schultz, A. J.; Teller, R. G.; Beno, M. A.; Williams, J. M.; Brookhart, M.; Lamanna, W.; Humphery, M. B. *Science* **1983**, *220*, 197

(10) (a) Koga, N.; Obara, S.; Morokuma, K. *J. Am. Chem. Soc.* **1984**, *106*, 4625. (b) Koga, N.; Morokuma, K. *J. Am. Chem. Soc.* **1988**, *110*, 108. (c) Koga, N.; Morokuma, K. *J. Am. Chem. Soc.* **1993**, *115*, 6883. (e) Musaev, D. G.; Morokuma, K. *J. Am. Chem. Soc.* **1995**, *117*, 799. (f) Koga, N.; Morokuma, K. *Chem. Rev.* **1991**, *91*, 823. (e) Zeigler, T.; Folga, E.; Berces, A. *J. Am. Chem. Soc.* **1993**, *115*, 636. (f) Folga, E.; Zeigler, T. *Can. J. Chem.* **1992**, *70*, 333.

(11) (a) Benson, M. T.; Cundari, T. R.; Moody, E. W. *J. Organomet. Chem.* **1995**, *504*, 1. (b) Cundari, T. R.; Matsunaga, N.; Moody, E. W. *J. Phys. Chem.* **1996**, *100*, 6475. (c) Gordon, M. S.; Cundari, T. *Coord. Chem. Rev.* **1996**, *147*, 87. (d) Janiak, C. *J. Organomet. Chem.* **1995**, *501*, 219. (e) Carroll, J. J.; Haug, K. L.; Weisshaar, J. C.; Blomber, M. R. A.; Siegbahn, P. E. M.; Svensson, M. *J. Phys. Chem.* **1995**, *99*, 13955. (f) Siegbahn, P. E. M.; Crabtree, R. H. *J. Am. Chem. Soc.* **1996**, *118*, 4442. (g) Re, N.; Rosi, M.; Sgamellotti, A.; Floriani, C.; Guest, M. F. *J. Chem. Soc., Dalton Trans.* **1993**, 1821.

(12) (a) Sargent, A. L.; Hall, M. B. *Inorg. Chem.* **1992**, *31*, 317. (b) Sargent, A. L.; Hall, M. B.; Guest, M. F. *J. Am. Chem. Soc.* **1992**, *114*, 517. (c) Song, J.; Hall, M. B. *J. Am. Chem. Soc.* **1993**, *115*, 327. (d) Ziegler, T.; Tschinke, V.; Liangyou, F.; Becke, A. D. *J. Am. Chem. Soc.* **1989**, *111*, 9177. (e) Musaev, D. G.; Morokuma, K. *J. Organomet. Chem.* **1995**, *504*, 93. (f) Lin, Z.; Hall, M. B. *J. Organomet. Chem.* **1994**, *478*, 197. (g) Jiménez-Cataño, R.; Hall, M. B. *Organometallics* **1996**, *15*, 1889. (h) Siegbahn, P. E. M. *J. Am. Chem. Soc.* **1996**, *118*, 1487.

Scheme 2

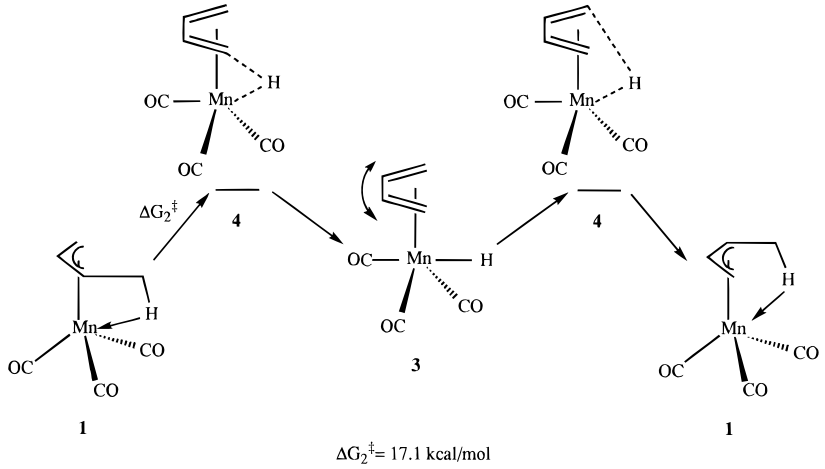

(CO) with Hartree−Fock and perturbation theory methods.[12c] Ziegler *et al.* studied this system as well by density functional theory.[12d] Musaev and Morokuma used restricted Hartree−Fock and second-order Møller−Plesset perturbation theory to study the reactivity of *trans*-RhCl(CO)$(PH_3)_2$ toward H_2, CH_4, and other molecules.[12e] Lin and Hall examined the role of the agostic bond in alkane activation in their study of the β-agostic to olefin−hydride isomerization in [CpRh-$(C_2H_4)(\eta^2$-$C_2H_5)]^+$.[12f] Jiménez-Cataño and Hall examined the inter- versus intramolecular C−H bond activation in rhodium and iridium complexes.[12g] Most recently, Siegbahn reported a theoretical study on the reactivity exhibited by CpMCO toward methane, where M = Co, Rh, Ir.[12h] Of interest was the cobalt complex's inability to activate methane. This is in contrast to its homologues, rhodium and iridium, both of which readily activate C−H bonds in methane. Siegbahn used a scaling scheme as well as perturbative methods and density functional theory. He reports achieving good agreement with available experimental data.

In this work, we describe a theoretical study of the fluxional behavior displayed by $(C_4H_7)Mn(CO)_3$. The presence of a first-row metal in the system requires a higher level of electron correlation as does accurate calculation of the small energetic differences involved in the isomerizations. First-row transition metals often present a more formidable challenge due to the compact nature of the d-orbitals. Preliminary calculations showed that methods conventionally used in second- or third-row transition metal systems would be inadequate for treating a first-row metal system. As we will show, an *ab initio* study of $(C_4H_7)Mn(CO)_3$ will provide additional insight into the theoretical treatment of a first-row metal system. Identification of transition states and intermediates as well as calculation of the energetics of the entire system will provide additional insight into the mechanism whereby the isomerizations in (C_4H_7)-$Mn(CO)_3$ occur.

Theoretical Details

Geometries were initially optimized for **1** and **3** as preliminary results indicated that **2** represented a transition state. For the geometry optimizations, the Hartree−Fock self-consistent field method (HF-SCF),[13] second-order Møller−Plesset perturbation theory (MP2),[14] and density functional theory (DFT)[15] were used. In the course of the HF-SCF geometry optimization of the $(\eta^4$-$C_4H_6)MnH(CO)_3$ intermediate (**3**), which is composed of two neutral fragments, no minimum was found for any Mn−C_4 fragment distance. Three different correlation functionals were used in conjunction with Becke's hybrid exchange potential (B3):[16] Lee−Yang−Parr (LYP),[17] Perdue (P86),[18] and Perdue−Wang (PW91).[19] As there were few differences among the equivalent DFT geometries, the P86 correlation functional was chosen on the basis that it provided the best convergence behavior. In the butadiene intermediate (**3**), C_s symmetry was imposed on the structure. No symmetry constraints are present in any other structures. In all geometry calculations, the C−O bond distances were fixed at 1.14 Å, the equilibrium distance from the crystal structure of **5**. The Mn−C−O bond angles were also fixed at 180°. Preliminary studies showed that the Mn−C−O bond angles deviated only slightly from linearity in a full optimization. Constraining the Mn−C−O bond angles introduces six imaginary frequencies in the minimum structures (**1** and **3**). These imaginary frequencies arise from the fact that at 180°, both Mn−C−O bending modes have negative force constants. These negative force constants give rise to second-order saddle points for each Mn−C−O bending mode. In any transition state structure (**2** and **4**, where **4** represents a transition state in the isomerization of **1** to **3**), we would expect to find one additional negative frequency. Quadratic synchronous transit calculations between minima were performed by DFT/B3P86 to identify preliminary transition state structures for **2** and **4**. Frequency calculations performed on these structures confirmed that each structure had one additional imaginary frequency and, therefore, that each represented a transition state.

Three basis sets were used in these calculations. The first (BSI) contains the ECP basis set of Hay and Wadt[20] for Mn and the double-ζ basis sets[21] for carbon, oxygen, and hydrogen, with ECPs[22] on C and O. The Mn basis set (55, 5, 5) was uncontracted to (541, 41, 41). This is not the basis set

(13) (a) Roothaan, C. C. *Rev. Mod. Phys.* **1951**, *23*, 69. (b) Roothaan, C. C. *Rev. Mod. Phys.* **1960**, *32*, 179.
(14) Møller, C.; Plesset, M. S. *Phys. Rev.* **1936**, *46*, 618.
(15) (a) Hohenberg, P.; Kohn, W. P *Phys. Rev.* **1964**, *136*, B864. (b) Kohn, W.; Sham, L. J. *Phys. Rev.* **1965**, *140*, A1133.
(16) (a) Becke, A. D. *Phys. Rev.* **1988**, *A38*, 3098. (b) Becke, A. D. *J. Chem. Phys.* **1993**, *98*, 1372. (c) Becke, A. D. *J. Chem. Phys.* **1993**, *98*, 5648.
(17) Lee, C.; Yang, W.; Parr, R. G. *Phys. Rev.* **1988**, *B37*, 785.
(18) Perdue, J. P. *Phys. Rev. B* **1986**, *33*, 8822.
(19) Perdue, J. P.; Wang, Y. *Phys. Rev. B* **1991**, *45*, 13244.
(20) Hay, P. J.; Wadt, W. R. *J. Chem. Phys.* **1985**, *32*, 299.
(21) Dunning, T. H.; Hay, P. J. *Modern Theoretical Chemistry*; Plenum: New York, 1976; Chapter 1, pp 1−28.

designated LANL2DZ in the GAUSSIAN-94[23] suite of programs, but a different contraction of the same primitive functions. Results obtained using the contraction given above differ from the LANL2DZ results by no more than 2 kcal/mol. The second and third basis sets (BSIIA and BSIIB) include polarization functions on selected carbons and hydrogens as well as manganese. The *p*-function for hydrogen ($\alpha = 0.2768$) and *f*-function for Mn ($\alpha = 2.185$) were optimized at the CISD level for Mn−H. The *d*-function for carbon ($\alpha = 0.5453$) was optimized at the CISD level for MnCH. BSIIA was used for the lower energy process, and polarization functions were placed on manganese, the agostic carbon (C_1), and the three potentially agostic hydrogens (H_{1a}, H_{1b}, H_{1c}). BSIIB was used for the higher energy process, and polarization functions were placed on manganese and all four butenyl carbons (C_{1-4}), but only the one hydrogen (H_{1a}) that forms the agostic bond in the ground state and the Mn−H bond in the η^4-intermediate. In each process, energies were calculated for the agostic ground state as well as the relevant species in the reaction path.

Energies obtained at the same level of calculation as the geometry optimizations were not accurate. At the DFT level, the difference in energy between **1** and **2** in the lower energy process was 0.69 kcal/mol, compared to $\Delta G^{\ddagger} = 9.1$ kcal/mol experimentally. The ΔE value for **1** and **4** was 23.2 kcal/mol, compared to $\Delta G^{\ddagger} = 17.1$ kcal/mol. The energy difference between the ground state (**1**) and the butadiene intermediate (**3**) at the DFT level was 21.6 kcal/mol. At the MP2 level, the energy difference between **1** and **3** was 7.0 kcal/mol, but comparison of the HF-SCF, MP2, and MP3 energies obtained at the MP2 geometry did not reveal a convergent series. The quadratic configuration interaction method that includes single and double excitations (QCISD)[24] as well as a perturbational estimate of the contribution of the triple excitations (QCISD(T))[25] was then used. In the QCI calculations, the 14 lowest-lying core orbitals were left uncorrelated, as were the 21 highest-lying virtual orbitals. The 14 low-lying core orbitals are the Mn 3s and 3p orbitals and the 2s orbitals on all carbons and oxygens. The truncation in the virtual space was performed based on the energy separation between shells of orbitals. The excluded virtual orbitals have the same qualitative character in the calculations with and without polarization functions. This result indicates that the orbitals created by the addition of the polarization functions are included in the correlated calculations with the larger basis sets.

All calculations were carried out with the GAUSSIAN-94[23] suite of programs. Calculations were performed on SGI-Indigo II series workstations, the SGI-Power Challenge at Texas A&M University, and the IBM-SP2 at the Cornell Theory Center.

Results and Discussion

Geometry Optimizations. Geometries were initially optimized for **1** and **3** at the HF, MP2, and DFT levels. The HF structures were unsatisfactory, as described above, and will not be discussed further. Since the experimental structure of **1** is unknown, the MP2 and DFT calculated geometries for **1** will be compared with the X-ray and neutron diffraction structures for **5**.[26] While the systems are not the same, there are sufficient similarities such that comparisons should be valid. Both the DFT/B3P86 and MP2 calculated structures for **1** (Figure 1) have the same pseudo-octahedral coordination about the Mn center observed in the experimental structure of **5**, in which the agostic hydrogen occupies a position *trans* to a carbonyl group. In the MP2 structure, however, the carbonyl ligands are overbound (see Table 1). The average Mn−CO distance in the neutron diffraction structure of **5** is 1.809(7) Å, whereas the average MP2 calculated distance is 1.72 Å. The neutron diffraction structure has an average Mn−C distance for the C_4 fragment of 2.12(6) Å, compared to the MP2 calculated distance in **1** of 2.1(1) Å. The strength of the agostic interaction is also overestimated somewhat at the MP2 level. In the neutron diffraction structure of **5**, the Mn−H_{1a} distance is 1.84(1) Å and the MP2 calculated value is 1.82 Å. The differences between the crystal structure measurements and those calculated with the MP2 method are more likely a result of the tendency of MP2 to overcorrect, relative to the HF-SCF behavior. Fragments that appear too weakly bound at the uncorrelated level are often overbound at the MP2 level. Overbinding is not observed within the C_4 fragment, however. Here, the C−C and C−H bonds vary from 0.03 to 0.05 Å too long. It is interesting, however, that the MP2 structure does have the correct agostic C_1−H_{1a} distance, when compared to the neutron diffraction data. The inconsistencies observed in the measurements of the rest of the allyl fragment may be attributed to the fact that we are comparing a C_6 ring to a C_4 fragment.

The geometry obtained at the DFT level for **1** appears to be in much better overall agreement with the experimental geometry for **5** than the MP2 structure. The average calculated Mn−C distance for the butenyl fragment for DFT/B3P86 is 2.2(1) Å, compared to 2.12-

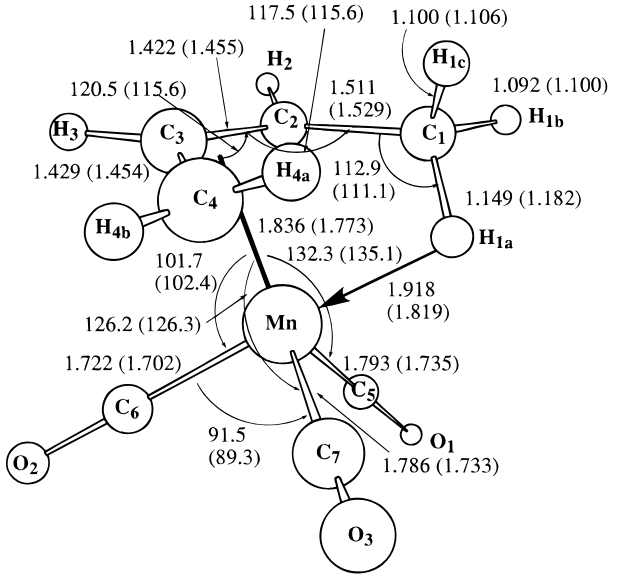

Figure 1. Optimized geometry of **1**, the agostic ground state of $(C_4H_7)Mn(CO)_3$. Bond distances are in Angstroms, and bond angles are in degrees. DFT/B3P86 values are given first, MP2 values are given in parentheses. The bold line from Mn to the centroid of C_2−C_3−C_4 terminates at the point Ω.

(22) Stevens, W. J.; Basch, H.; Krauss, M. *J. Chem. Phys.* **1984**, *81*, 6026.

(23) Frisch, M. J.; Trucks, G. W.; Head-Gordon, M.; Gill, P. M. W.; Wong, M. W.; Foresman, J. B.; Johnson, B. G.; Schlegel, H. B.; Robb, M. A.; Replogle, E. S.; Gomperts, J. L.; Andres, J. L.; Raghavachari, K.; Binkley, J. S.; Gonzales, C.; Martin, R. L.; Fox, D. J.; Defrees, D. J.; Baker, J.; Stewart, J. J. P.; Pople, J. A. *GAUSSIAN-94*; Gaussian, Inc.: Pittsburgh, PA, 1992.

(24) Pople, J. A.; Head-Gordon, M.; Raghavachari, K. *J. Chem. Phys.* **1987**, *87*, 5968.

(25) Pople, J. A.; Head-Gordon, M.; Raghavachari, K. *J. Chem. Phys.* **1987**, *87*, 5968.

(26) Schultz, A. J.; Teller, R. G.; Beno, M. A.; Williams, J. M.; Brookhart, M.; Lamanna, W.; Humphrey, M. B. *Science* **1983**, *220*, 197.

Table 1. Comparison between Geometry Parameters in the Calculated Structures of the $C_4H_7Mn(CO)_3$ Agostic Ground State (1) and Experimental Structures of the $CH_3C_6H_8Mn(CO)_3$ Agostic Ground State (5)[a]

parameter	**1**, MP2 geometry	**1**, B3P86 geometry	**5**, neutron structure	**5**, X-ray structure
$Mn-C_5$	1.735	1.793	1.809(7)[b]	1.805(3)
$Mn-C_6$	1.702	1.722	1.809(7)[b]	1.775(3)
$Mn-C_7$	1.733	1.786	1.809(7)[b]	1.814(3)
C_1-C_2	1.529	1.511	1.535(5)	1.485(3)
C_1-H_{1c}	1.106	1.100		
C_1-H_{1a}	1.182	1.149	1.19(1)	1.07(2)
C_1-H_{1b}	1.100	1.092		1.03(2)
C_2-C_3	1.455	1.422	1.41(1)[b]	1.385(4)
C_3-C_4	1.454	1.429	1.41(1)[b]	1.400(4)
$Mn-C_1$	2.283	2.368	2.34(1)	2.301(2)
$Mn-C_2$	1.984	2.024	2.12(6)	2.053(3)
$Mn-C_3$	2.119	2.127	2.12(6)	2.092(2)
$Mn-C_4$	2.105	2.158	2.12(6)	2.168(3)
$Mn-H_{1a}$	1.819	1.914	1.84(1)	1.86(2)
$Mn-\Omega$	1.773	1.836		
C_5-Mn-C_6	87.4	89.9		87.5(1)
C_5-Mn-C_7	97.1	99.1		100.8(1)
$C_5-Mn-\Omega$	135.1	132.3		
C_6-Mn-C_7	89.3	91.5		90.4(1)
$C_6-Mn-\Omega$	102.4	101.7		
$C_7-Mn-\Omega$	126.3	126.2		
$C_2-C_1-H_{1c}$	113.7	113.1		
$C_2-C_1-H_{1a}$	111.1	112.9		113(1)
$C_2-C_1-H_{1b}$	112.1	112.1		111(1)
$C_1-C_2-C_3$	115.6	117.5		114.3(2)
$C_2-C_3-C_4$	115.6	119.0		116.9(2)
$H_{1c}-C_1-C_2-C_3$	−49.0	−54.3		
$H_{1a}-C_1-C_2-C_3$	65.9	61.5		
$H_{1b}-C_1-C_2-C_3$	−177.0	180.0		
$C_1-C_2-C_3-C_4$	−21.9	−17.0		

[a] Ω refers to the centroid of the $C_2-C_3-C_4$ unit. r(C−O) is fixed at 1.14 Å. Bond lengths are in angstroms, and bond angles and torsion angles are in degrees. [b] Average value.

(6) Å for the neutron diffraction structure. The average calculated Mn−CO distance is 1.784(8) Å, compared to 1.809(7) Å in the neutron diffraction structure. The DFT calculation underestimates the agostic interaction, however. The calculated $Mn-H_{1a}$ distance is 1.92 Å, and in the neutron structure of **5** it is 1.84(1) Å. Likewise, the C_1-H_{1a} distance is shorter in the DFT structure than it is in the neutron diffraction crystal structure. This disparity is consistent with DFT's underestimation of the strength of the agostic bond due to the significant dispersion contribution in this type of interaction. Similar accuracy in bond angles is observed in the DFT structure and the MP2 structure. Differences from the crystal structure of **5** are no more than 2°. Overall, the DFT structure seems more accurate for stronger Mn−L bonds.

For the intermediate, **3**, while there is no known experimental structure, we can compare the MP2 and DFT/B3P86 structures (Figure 2) and their distortion from the agostic ground state structures. Most notable is the formation of the Mn−H bond. The distances calculated in both methods are shorter than observed Mn−H bonds. The MP2 distance is shorter at 1.51 Å than the DFT distance at 1.56 Å, while a typical Mn−H distance, as in $HMn(CO)_5$ is 1.601(16) Å. The two structures are alike in this regard, but differ in almost all others.

Most notable are the changes in the Mn−CO bond distances and the changes in the angles in the pseudo-octahedral coordination sphere about the metal center.

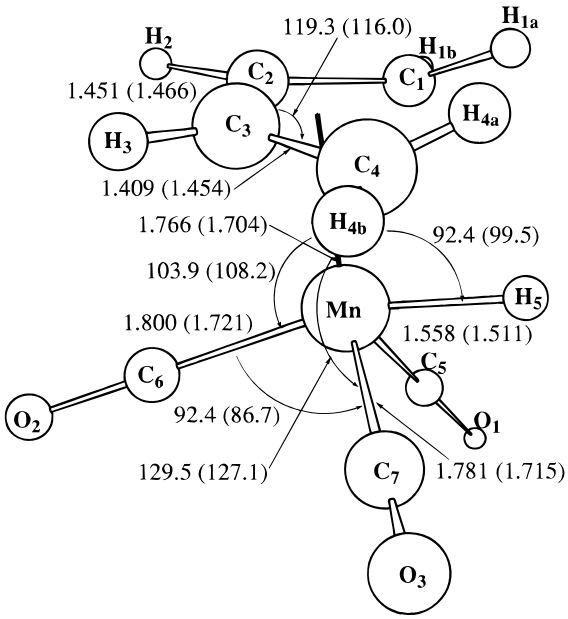

Figure 2. Optimized geometry of **3**, the intermediate in Scheme 2, (η^4-C_4H_6)$MnH(CO)_3$. Bond distances are in Angstroms, and bond angles are in degrees. DFT/B3P86 values are given first, MP2 values are given in parentheses. The bold line from Mn to the centroid of $C_1-C_2-C_2-C_4$ terminates at the point Ω.

A common occurrence in transition metal hydride complexes is the contraction of a metal−carbonyl bond *trans* to the hydride, relative to the other bonds in the same complex.[27] This is observed in both calculated geometries of **1**, as well as the experimental structures of **5**, and in the DFT structure of **3**. However, in the MP2 geometry of **3**, this shortening is absent and, in fact, there is a slight difference in the other direction. The carbonyl groups in the MP2 structure all remain overbound with an average distance of 1.72 Å, and there is only a small difference between the Mn−CO bond *trans* to the hydride and those that occupy the *cis* positions.

Different changes in the coordination sphere are also observed in the comparison between the MP2 and DFT structures in the isomerization of **1** to **3**. The angles between the *cis* and *trans* carbonyls of **3** are more acute in the MP2 structure than in the DFT structure. In the comparison of **1** and **3**, the average *cis*-,*trans*-carbonyl angle opens in the DFT isomerization from 90.7° in **1** to 92.4° in **3**, while between the MP2 structures, the change is of the same magnitude (from 88.4° in **1** to 86.7° in **3**) but in the opposite direction. The angle between the two *cis*-carbonyls (C_5-Mn-C_7), in contrast, opens in the MP2 process from 97.1° in **1** to 103.7° in **3**, while in the DFT geometries, the same angle closes slightly from 99.1° to 96.3°. Thus, the DFT structures appear to maintain the octahedral environment around the metal upon isomerization more so than the MP2 structures.

QCISD calculations were then used to compare the B3P86 geometries with the analogous MP2 geometries to establish which set should be used for more expensive transition state optimizations, frequency calculations,

(27) (a) LaPlaca, S. J.; Hamilton, W. C.; Ibers, J. A.; Davidson, A. *Inorg. Chem.* **1969**, *8*, 1928. (b) Frenz, B. A.; Ibers, J. A. In *Transition Metal Hydrides*; Muetterties, E. L., Ed.; Marcel Dekker: New York, 1971; pp 41−43.

Table 2. Geometry Parameters of the Calculated Structures in the $C_4H_7Mn(CO)_3$ System[a]

parameter	**3**, MP2 geometry	**3**, B3P86 geometry	**2**, B3P86 geometry	**4**, B3P86 geometry
$Mn-C_5$	1.715	1.872	1.790	1.783
$Mn-C_6$	1.721	1.800	1.756	1.820
$Mn-C_7$	1.715	1.872	1.788	1.762
C_1-C_2	1.454	1.409	1.531	1.414
C_1-H_{1c}			1.096	
C_1-H_{1a}	1.094	1.084	1.100	1.087
C_1-H_{1b}	1.096	1.087	1.100	1.086
C_2-C_3	1.466	1.451	1.423	1.451
C_3-C_4	1.454	1.409	1.429	1.418
C_1-H_5	2.411	2.394		2.278
$Mn-C_1$	2.104	2.139	2.802	2.200
$Mn-C_2$	2.157	2.223	2.129	2.138
$Mn-C_3$	2.157	2.223	2.113	2.169
$Mn-C_4$	2.104	2.139	2.118	2.230
$Mn-H_5$	1.511	1.558		1.581
$Mn-\Omega$	1.704	1.766	1.833	1.756
$\Omega-Mn-H_5$	99.5	92.4		107.4
C_5-Mn-C_6	86.7	92.4	89.9	83.7
C_5-Mn-C_7	103.7	96.3	100.0	96.5
$C_5-Mn-\Omega$	127.1	129.5	128.8	133.5
C_6-Mn-C_7	86.7	92.4	90.9	94.8
$C_6-Mn-\Omega$	108.2	103.9	102.8	101.3
$C_7-Mn-\Omega$	127.1	129.5	128.7	128.6
$C_2-C_1-H_{1c}$			112.6	
$C_2-C_1-H_{1a}$	120.8	121.7	113.7	120.5
$C_2-C_1-H_{1b}$	116.7	118.7	108.8	120.0
$C_1-C_2-C_3$	116.0	119.3	122.2	118.6
$C_2-C_3-C_4$	116.0	119.3	120.8	122.8
$H_{1c}-C_1-C_2-C_3$			−0.6	
$H_{1a}-C_1-C_2-C_3$	42.6	35.7	123.2	−33.4
$H_{1b}-C_1-C_2-C_3$	−169.3	−169.2	−119.0	170.1
$C_1-C_2-C_3-C_4$	0.0	0.0	35.7	−5.47

[a] Ω refers to the centroid of the $C_2-C_3-C_4$ unit in **2** and the $C_1-C_2-C_3-C_4$ in **3** and **5**. r(C−O) is fixed at 1.14 Å. Bond lengths are in Angstroms, bond angles and torsion angles are in degrees.

Table 3. Comparison of QCISD and QCISD(T) Energies (au) for 1 and 3 in BSI

	QCISD// MP2	QCISD// B3P86	QCISD(T)// B3P86
1	−193.302 517 8	−193.334 404 8	−193.357 073 1
3	−193.254 576 1	−193.296 797 7	−193.320 521 1
ΔE (kcal/mol)	30.08	23.60	22.94

and more highly correlated energy calculations (Table 3). The QCISD calculations revealed that the B3P86 geometries were not only both lower in energy than the corresponding MP2 geometries (**1** $E = -193.3344048$ vs -193.3025178; **3** $E = -193.2967977$ vs -193.2545761) but also that the energy difference between the two B3P86 structures at the QCISD level was much closer to the experimental value. Since the QCISD total energies showed that the DFT/B3P86 geometries for **1** and **3** are more accurate, the transition state geometries were obtained for both Scheme 1 and Scheme 2 by DFT/B3P86.

In the lower energy process, Scheme 1, the agostic ground state has the methyl group bent below the plane of the other three carbons by approximately 20°, such that it can interact with the metal. During the course of the isomerization, the agostic bond to the metal is broken and the methyl group moves above the plane of the other carbon atoms by 36°. The upward motion of the methyl group produces the transition state, **2** (Figure 3). The methyl group also rotates approximately 50° and opens the $C_1-C_2-C_3$ angle from 117.5° to 122.2°. No agostic interaction is present in this

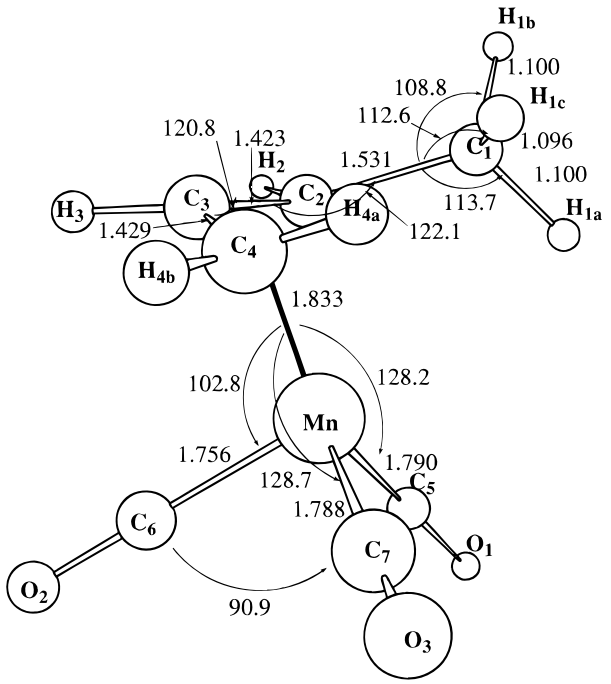

Figure 3. DFT/B3P86-optimized geometry of **2**, the transition state in Scheme 1, (η^3-C_4H_7)$Mn(CO)_3$. Bond distances are in Angstroms, and bond angles are in degrees. The bold line from Mn to the centroid of $C_2-C_3-C_4$ terminates at the point Ω.

complex. The absence of the agostic interaction is further supported by the lengthening of the Mn−CO bond distance *trans* to the agostic site.

In the higher energy process, Scheme 2, the η^4-butadienyl intermediate, **3**, is formed. In the transition state for this process, **4** (Figure 4), the hydrogen has nearly completed its migration to the metal as the metal-hydride distance is only 0.03 Å longer in the transition state than it is in the intermediate. The calculated metal-carbonyl distances for **4** fall between those for **1** and **3**. The C_4 fragment clearly shows a transition between η^3-butenyl and η^4-butadienyl character. The agostic carbon C_1-C_2 distance shortens from 1.511 to 1.414 Å between the agostic ground state and the transition state. The C_3-C_4 distance shows the same behavior, shortening from 1.429 to 1.418 Å. The C_2-C_3 bond, accordingly, lengthens from 1.422 to 1.451 Å. The values for the η^4-intermediate are $r(C_1-C_2) = 1.409$ Å and $r(C_2-C_3) = 1.451$ Å. The proximity of the transition state's values to those calculated for the intermediate indicates that the transition state falls late in the reaction path, closer to the intermediate than to the ground state. The connection of **4** to both **1** and **3** was confirmed *via* an internal reaction coordinate (IRC) calculation in which we followed the reaction off the transition state in both directions.

Frequency calculations were performed on **1**, **2**, **3**, and **4** at the DFT/B3P86 level to ensure that the geometries obtained were indeed minima and first-order saddle points, as appropriate. No negative frequencies were found for either **1** or **3**, apart from those introduced by the geometrical constraint in both molecules that the Mn−C-O bond angles be 180°. In the transition states, **2** and **4**, each structure has one additional imaginary frequency.

Reaction Energetics. Although energies were obtained at the QCISD level in BSI for both MP2 and DFT

Table 4. QCISD/BSII Energies, Zero-Point Energy and Temperature Corrections, and Theoretical Free Energies (au)

	QCISD (BSII)	correction (DFT/BSI)	G_{theor}	G_{exp}
1	−193.420 72 (IIA)	0.0920 00	−193.254 77	
	−193.528 78 (IIB)		−193.362 83	
3	−193.503 65 (IIB)	0.0886 17	−193.340 91	
2	−193.406 22 (IIA)	0.0909 23	−193.240 72	
4	−193.493 82 (IIB)	0.0845 27	−193.409 29	
1 to **2**	9.10 kcal/mol (IIA)		$\Delta G^{\ddagger}$ = 8.43 kcal/mol	$\Delta G^{\ddagger}$ = 9.1 kcal/mol
1 to **3**	15.8 kcal/mol (IIB)		ΔG = 13.7 kcal/mol	
1 to **4**	21.0 kcal/mol (IIB)		$\Delta G^{\ddagger}$ = 17.2 kcal/mol	$\Delta G^{\ddagger}$ = 17.1 kcal/mol

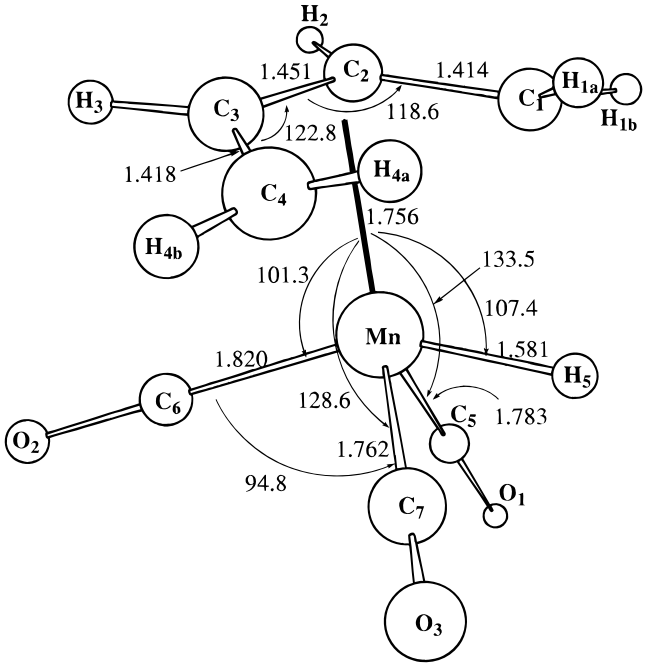

Figure 4. DFT/B3P86-optimized geometry of **4**, the transition state in Scheme 2. Bond distances are in Angstroms, and bond angles are in degrees. The bold line from Mn to the centroid of $C_1-C_2-C_2-C_4$ terminates at the point Ω.

geometries of **1** and **3**, as described in the theoretical details, subsequent energy calculations were performed only on the DFT/B3P86 structures. The energy differences between the two minimum structures, **1** and **3**, were calculated with QCISD and QCISD(T) methods (Table 3). QCISD(T) calculations were performed in BSI. In these results, neither the energies nor the energy difference between them changes greatly with the addition of the triple excitation contribution to the QCISD calculation (ΔE = 23.60 vs 22.94 kcal/mol). We take this as an indicator that the triple excitation contributions are not important for the calculation of the energy differences in this system. However, the calculated ΔE is still inaccurate compared to the experimental value for the barrier.

QCISD calculations were then performed in BSII, which includes polarization functions. Energy differences calculated at this level gave very satisfactory results (Table 4). The calculated energies for the species in the processes supported the proposed mechanisms. The activation energy for Scheme 1 (**1** to **2**, calculated in BSIIA) is 9.10 kcal/mol. The activation energy for Scheme 2 (**1** to **4**, calculated in BSIIB) is 21.0 kcal/mol. The energy difference between the two minima (**1** to **3**, calculated in BSIIB) is 15.77 kcal/mol. This indicates that there exists a shallow energy well for the intermediate (**3**). Since the calculated changes in total electronic energy cannot be directly compared with the experimentally obtained $\Delta G^{\ddagger}$ values, temperature corrections and zero-point energies have also been calculated to obtain the free energy values for the complexes (see Table 4). To the zero-point corrected energies we add the temperature corrections at room temperature for $H + TS$. From these calculations, $\Delta G^{\ddagger}_{theor}$ for Scheme 1 is 8.42 kcal/mol. ΔG_{theor} between the agostic ground state (**1**) and the intermediate (**3**) in Scheme 2 is 13.7 kcal/mol, and $\Delta G^{\ddagger}_{theor}$ for Scheme 2 is 17.2 kcal/mol.

Conclusions

In this work, we have demonstrated what level of theory is necessary to treat fluxional processes in a system that contains both an agostic interaction and an oxidative addition as well as a first-row transition metal. We have found QCISD energy differences obtained for DFT geometries, in a basis set containing polarization functions, to be accurate to within 1 kcal/mol. Geometries obtained at the density functional level compared favorably with an available experimental structure. Bond distances typically differed by no more than 0.05 Å and were, for the most part, much closer. Angles in the structures varied by no more than 3°. The accuracy of DFT calculations with the B3P86 functional was better than that of MP2 for the geometries in the system. Experimental free energies of activation were $\Delta G^{\ddagger}$ = 9.1 kcal/mol for Scheme 1 and $\Delta G^{\ddagger}$ = 17.1 kcal/mol for Scheme 2. Computed values were 8.43 kcal/mol and 17.2 kcal/mol, respectively. We have found this combination of methods to be accurate without being excessively time-consuming.

Acknowledgment. The authors would like to thank the National Science Foundation (Grant No. CHE 94-13634) for financial support. J.L.C.T. would like to thank Dennis Marynick for helpful discussions and the National Aeronautics and Space Administration for financial support (NGT-51337). This research was conducted in part with use of the Cornell Theory Center, a resource for the Center for Theory and Simulation in Science and Engineering at Cornell University, which is funded in part by the National Science Foundation, New York State, and IBM Corp.

Supporting Information Available: A table containing the total energies of **1**, **2**, **3**, and **4** at the B3P86 level (1 page). Ordering information is given on any current masthead page.

OM9701229